19

Two-Step Sintering Applied to Ceramics

Gislâine Bezerra Pinto Ferreira, José Ferreira da Silva Jr,
Rubens Maribondo do Nascimento, Uílame Umbelino Gomes
and Antonio Eduardo Martinelli
Federal University of Rio Grande do Norte
Brazil

1. Introduction

During the process of sintering of ceramics, it is necessary to apply high temperature owing the high melting point of the raw materials. In general, a ceramist, wishing to produce a material with particular properties, must identify the required microstructure and then design processing conditions that will produce this required microstructure (Lutgard et al., 2003). One of the options to adapt the microstructure is a technique called two step sintering (TSS), this technique has been applied to the sintering of ceramic oxides to achieve full density without grain growth in final stage of sintering without loss densification (Chen & Wand, 2000). The two-step sintering process consists in to heat a ceramic body to a peak temperature (T1) to achieve an intermediate density and then the temperature is reduced to a dwell temperature (T2), which is held till full density is achieved. To succeed in two-step sintering, a sufficiently high relative density (70% or greater) needs to be achieved at T1 (Chen & Wang, 2000 & Chen, 2000). Once this critical density is reached, a lower temperature, T2, used for the isothermal hold will be sufficient to achieve full density. Difference between kinetics of grain boundary diffusion and grain boundary migration is used to obtain almost full dense, nanostructured ceramics. During the last stage of the sintering occur the grain growth in materials, this implicate in final properties, like mechanical resistance, density, ionic and electrical conductivity and others (Robert et al., 2003). The two-step sintering has been applied in many mateirals with the main goal of avoiding the grain growth in final stage of sintering, the results show the TSS is a technique efficient for it. Some application for two-step sintering are materials which need high density and small grain size, for example electrolytes of solid oxide fuel cell, as ceramics based in Y_2O_3 and CeO_2, both with and without doppant (Wang et al., 2006; Wright, 2008 & Lapa, 2009). Others examples in which TSS are used also as nanostructural fosterite (Fathi, et al., 2009), alumina-zirconia ceramics (Wang et al., 2008), TiBaO3 and Ni-Cu-Zn Ferrite (Wang et al., 2006), ZnO (Shahraki et al., 2010). In this cases, the researchs are getting the relative density higher than 97% and the size grains in level sub-micrometer.

2. Mechanisms of two-step sintering

During the process of the TSS the first step needs high temperature enough to achieve the critical diameter spherical (d_c) of the core to become the crystallization, in this step the

relative density (ρ) need be the same or higher than 75% of the teorical density to obtain unstable pores and the sintering the material be kept. In the second step is necessary the temperature to keep the densification until the end of the sintering, but avoiding the grain growth. An important reason to have an understanding of two-step sintering is the possibility to increase the heat rate of sintering, to avoid the grain growth and to obtain a material with improved mechanical, thermal, electrical and optical properties in the materials (Chen & Wang, 2000). The absence of grain growth in second-step sintering has important implications for kinetics. Grain coarsening creates a powerful dynamic that constantly refreshes the microstructure. Statistically, only one-eighth of all grains survive every time the size of the grains doubles. This evolution can be a source of enhanced kinetics. Even without grain growth, enhanced kinetics has also been suspected in cases when microstructure evolution is otherwise robust; for example, in fine-grain superplasticity (McFadden et al., 1999; Wakai et al., 1990 & Chen & Xue, 1990). Because second-step sintering proceeds in a ´frozen' microstructure, it should have slower kinetics. Yet the slower kinetics is sufficient for reaching full density, while providing the benefit of suppressing grain growth. The diffusion kinetics is quantified in the frozen microstructure by measuring the densification rates in the second step, and comparing them with the prediction based on Herring's dimensional argument (Herring, 1950) for normalized densification rate (dr/rdt, where r is relative density and t is time):

$$\frac{d\rho}{\rho dt} = F(\rho)\left(\frac{\gamma\Omega}{GkT}\right)\left(\frac{\delta D}{G^3}\right) \quad (1)$$

Here γ is surface energy, Ω is atomic volume, G is grain size, d is grain-boundary thickness, and D is grain-boundary diffusivity. In the above, $\gamma\Omega$/GkT may be viewed as the normalized driving force, and $\delta D/G^3$ is the standard kinetic factor that enters the strain-rate equation for grain-boundary processes such as sintering, diffusional creep and superplasticity. The remaining dimensionless prefactor on the right-hand side, F, is independent of the grain size as such, but could depend on other aspects of the microstructure such as density and pore distribution (Wei & Wang, 2000).

Grain boundaries in ceramics have been extensively investigated in recent years with the intent to understand their structures and mechanical/electrical properties. Grain boundaries are also important for kinetic phenomena, such as sintering, grain growth, diffusional creep and superplasticity. Their importance increases as the grain size decreases, since the ratio of grain boundary to the grain interior is inversely proportional to the grain size. In addition, this ratio also dictates that there is a large capillary pressure (and its variation) in fine grain materials. For a typical grain boundary energy (and surface energy) in ceramics of 1 J/m^2, the capillary pressure is of the order of 2000 MPa at a grain size of 1 nm, 200 MPa at 10 nm, and 20MPa at 100 nm. These pressures are rather significant and may cause additional kinetic effects at intermediate and high temperatures. In general, the dominant kinetic paths in submicron powders and ceramic bodies are surfaces and grain boundaries, the latter becoming increasingly important as the relative density reaches toward 100%. "Clean" experiments on grain boundary kinetics without the "contamination" of surface effects can be undertaken provided full density is first achieved. Common ceramic firing processes, however, always induce rapid grain growth when the relative density exceeds 85%, because of the breakdown of pore channels at three grain junctions and the resulting reduction of the pore drag on grain boundary migration. Nevertheless, the combination of good powder

processing, fine starting powders, and low sintering temperatures may help to achieve submicron grain sizes in fully dense bodies. Such ceramics are suitable for kinetic studies of grain boundaries (Chen, 2000). The feasibility of densification without grain growth relies on the suppression of grain-boundary migration while keeping grain boundary diffusion active. Two-step sintering can be used to achieve a relative density of 98% by exploiting the ''kinetic window' that separates grain-boundary diffusion and grain-boundary migration. When conditions for two-step sintering fall below the ''kinetic window,'' a density _ 96% cannot be achieved even if a starting density of 70% is achieved at T1, as grain growth may still be suppressed but densification will be exhausted. Above the ''kinetic window,'' grain growth is likely to occur (Wright, 2008). The suppression of the final-stage grain growth is achieved by exploiting the difference in kinetics between grain boundary diffusion and grain-boundary migration. Such a process should facilitate the cost-effective preparation of other nanocrystalline materials for practical applications. To succeed in two-step sintering, a suficiently high starting density should be obtained during the first step. When the density is above 70%, porosimetry data have shown that all pores in Y_2O_3 become subcritical and unstable against shrinkage (which occurs by capillary action). These pores can be called as long as grain-boundary diffusion allows it, even if the particle network is frozen as it clearly is in the second step (Chen & Wang, 2000). From the thermodynamics aspect, at a temperature range where grain boundary diffusion is active, but grain boundary migration is sufficiently sluggish, densification would continue without any significant grain growth. On basis of this idea was developed to suppress the accelerated grain growth at the final stage of sintering by triple junctions. To take the advantage of boundary dragging by triple junctions, a critical density at first should be achieved where sufficient triple junctions exist throughout the body as pins. Then with decreasing the sintering temperature to a critical degree, the grain growth would be stopped by triple junctions while densification may not be impaired. In doing so, samples have to be exposed to prolonged isothermal heating at the second (low temperature) step. As in a TSS regime, the triple junctions are going to prohibit grain growth, while unstable pores can shrink with low temperature annealing, seemingly the source of different densities lies in the pore size and distribution which needs to be further investigated. Certainly, formation of inhomogeneous porosity due to the increased tendency of nanopowder to form agglomerates complicates the situation. To solve this problem, one can use larger particles with lower agglomeration degree and shape green bodies with advanced methods to obtain a more homogenous structure. Under this condition, one can expect successful TSS at lower temperatures (Hesabi et al., 2008).

Sophisticated firing profiles are an alternative to compositional effects, to obtain dense ceramics with proper microstructure. Two-step sintering profiles, including optimized combinations of peak and dwell sintering temperatures, produced nanostructured materials with high densification at reasonably low temperatures, due to different grain growth and densification kinetics (Chen & Wang, 2000). Was observed that samples processed by two-step sintering show best results the density, around 94% of theoretical density and sub-micrometer grain size (Lapa, 2009).

3. Grain boundary kinetics during intermediate and final stage sintering

Sintering data are often used to infer the rate-controlling mechanism following the scaling analysis of Herring (Herring, 1950 & Herring, 1951).

$$\frac{d\rho}{dt} = \left(\frac{f(\rho)}{kTR^m}\right) D_0 \, exp(-Q/kT) \quad (2)$$

In the above, ρ is the relative density, m is either 3 for lattice diffusion or 4 for grain boundary diffusion, D_0 and Q refer to the pre-factor and activation energy of either lattice diffusion or grain boundary diffusion, and f is a constant that is dependent on the pore/grain geometry of the sintering body. Over a range of relative density, from 60% to 90%, some model calculations suggest that f is relatively constant (Coble, 1965 & Swinkels and Ashby, 1981). Thus, Eq. (2) can be used to deduce the diffusivity and the rate controlling mechanism if the densification rate and the grain size are known. In practice, plotting Log $(Td\rho=dt)R^m$ against $1/T$ usually yields a straight line regardless whether m is chosen as 3 or 4. This is due to the relatively poor resolution of such plotting method, the unavoidable scatter of the data, and the uncertainty of the value of $f(\rho)$. Therefore, it is usually not possible to definitively state that the sintering mechanism is via grain boundary diffusion or lattice diffusion based on the scaling analysis alone. On the other hand, the inferred values of diffusivities, and especially those of the activation energy, are usually quite different depending on whether m is chosen as 3 or 4. Thus, when independent diffusivity data are available, e.g., from grain boundary mobility measurements, a self-consistency check may be applied to infer whether the lattice or grain boundary mechanism applies. Using this method, is possible to conclude that later stage sintering of submicron CeO_2 and Y_2O_3 powders is controlled by grain boundary diffusion (Chen & Chen, 1997). As cited above, to achieve densification without grain growth, is necessary to first fire the ceramic at a higher temperature ($T1$) to a relative density of 75% or more, then sinter it at a lower temperature ($T2$) for an extended time to reach full density. This schedule is different from the conventional practice for sintering ceramics, in which the temperature always increases or, at least is held constant at the highest temperature, until densification is complete. The temperature $T2$ required for the second step decreased with the increasing grain size. However, if $T2$ is too low, then sintering proceeds for a while and then becomes exhausted. On the other hand, if $T2$ is too high, grain growth still occurs in the second step. Chen 2000, observed that the same shape in different Y_2O_3 but the medium temperature is shifted depending on the solute added. The results imply that grain boundaries previously stabilized at a higher temperature are difficult to migrate at a lower temperature even though they may still provide fast diffusion paths. The presence of impurity or solute segregation is not essential for this observation, since the same observation was found in pure Y_2O_3 as well as Y_2O_3 doped with both diffusion enhancing and diffusion-suppressing solutes. Therefore, the suppression of migration is not due to solute pinning. This suggests, for the first time that the mechanism for grain boundary migration is not grain boundary diffusion even in a pure substance. If the activation energy of the additional step is higher than that of grain boundary diffusion, it could explain why grain boundary migration is inhibited at low temperatures but not at high temperature. The most likely candidates for such step are movement of nodal points or nodal lines on the grain boundary, such as four-grain junctions, pore-grain boundary junctions, or three-grain junctions. The structures of these nodal points and lines may be special and they could become stabilized by prior high temperature treatment, rendering them difficult to alter to accommodate the subsequent movement of migrating grain boundary at low temperatures. Empirically, this may be modeled by assigning mobility to the nodal point (line), whose ratio to grain boundary mobility decreases with increasing temperature.

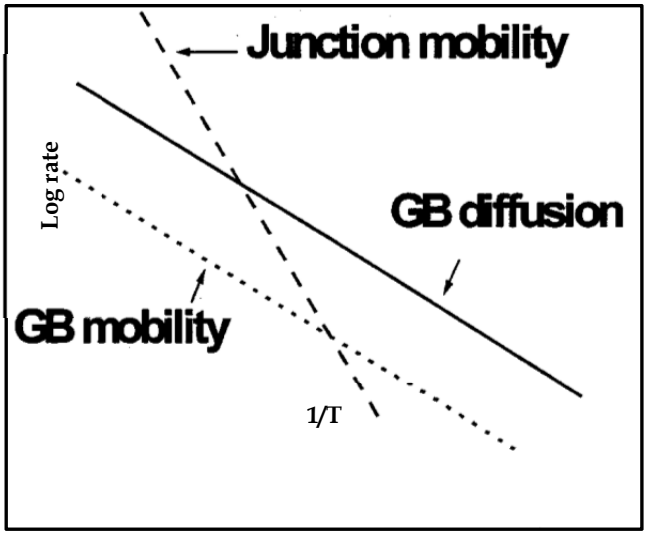

Fig. 1. Schematic Arrhenius plot for grain boundary diffusion, mobility of pore/grain-boundary junction or four-grain junction, and intrinsic mobility of grain boundary (without extrinsic drag due to nodal points/lines) (Source: Gary J. Wright, 2008).

Simple arguments then show that below a certain temperature, equilibrium grain boundary migration does not obtain since the boundaries are effectively pinned by the nodal points (lines). As mentioned above, enhanced grain boundary migration is often observed in superplastic deformation of fine grain oxides. The grain growth in this case is found to be controlled by the plastic strain. Indeed the ratio of grain size is essentially of the same order as the ratio of specimen dimensions before and after deformation (Chen & Xue, 1990). This may be regarded as opposite to the suppression of grain boundary migration described above. It is likely that in both cases, the dynamics of the nodal line/point are important. In superplasticity, the dynamics are enhanced to facilitate grain boundary migration. In low temperature sintering, the dynamics are inhibited to suppress grain boundary migration. A better knowledge of the structures of the grain boundary nodal points and lines, in both equilibrium configurations and in dynamic configurations would be required for a full understanding of the grain boundary kinetics. One interesting observation though is that a parallel effect of solute is seen in all three cases: normal grain growth, dynamic grain growth, and sintering without grain growth. For example, solutes that enhance normal grain growth also cause faster dynamic grain growth, and solutes that suppress normal grain growth likewise show a higher temperature $T2$ in the kinetic window for sintering without grain growth. Thus, while the kinetics of the nodal point/line may be distinct from that of grain boundary diffusion, they may not be entirely independent of each other. Recent studies of high-purity zinc have shown that grain-boundary migration can be severely hampered by the slow mobility of grain junctions at lower temperatures, the latter having a higher activation energy (Czubayko, et al., 1998). It is possible that a similar process, in which grain junctions as well as grain boundary/pore junctions impede grain-boundary migration, may here explain the apparent suppression of grain growth at lower temperatures. Interface kinetics in very fine grain polycrystals is sometimes limited due to

difficulties in maintaining sources and sinks to accommodate point defects 21±23. This leads to a threshold energy or stress, of the order of 2g/G. For a grain size of 100 nm, this amount to 20MPa, which is rather substantial compared to capillary pressure and could be the cause for the suppression. This effect should diminish at larger grain sizes, allowing the kinetic window to extend to lower temperatures. Therefore, in exploiting the difference in the kinetics of grain-boundary diffusion and grain-boundary migration to achieve densification without growth at lower temperatures, it is still advisable to utilize dopants to `tune' the overall kinetics.

4. Influence of triple junctions on grain boundary motion

According Czubayco et al., during the formation of granular structure of a polycrystalline material, both grain boundaries and triple junctions influence in characteristics. In the past, just the of grain boundaries motion were studied, while the influence of triple junctions on grain boundary has not attention necessary. In the last years, the velocity of the junction motion, the shape of the intersecting grain boundaries must be measured. Moreover, the steady-state motion of a grain boundary system with a triple junction is only possible in a very narrow range of geometrical boundary configurations. It is usually assumed that triple junctions do not influence the motion of the adjoining grain boundaries and that their role is reduced to control the thermodynamic equilibrium angles at the junction during the boundary motion. A specific mobility of triple junctions was first introduced by Shvindlerman and co-workers (Galina et al., 1987), who considered the steady-state motion of a grain boundary system with a triple junction. The geometry of the used boundary system is shown in Fig. 2. The boundaries of this system are perpendicular to the plane of the diagram, and far from the triple junction they run parallel to one another and to the x-axis.

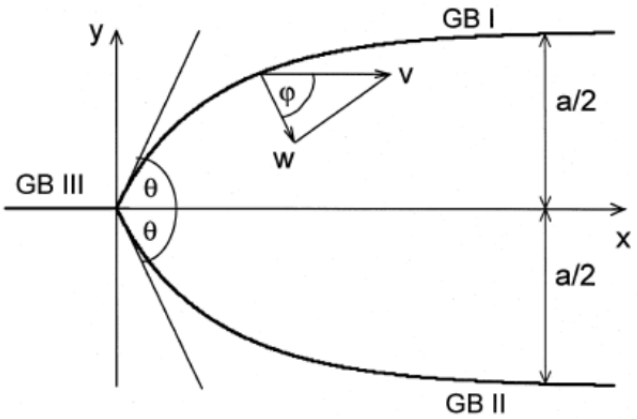

Fig. 2. Geometry of the grain boundary system with triple junction in the course of steady state motion (From: Czubayko et al., 1998).

The three boundaries of the system are considered identical, in particular their surface tension σ and their mobility m^{GB}. Furthermore, it is assumed that m^{GB} and σ are independent of the inclination of the grain boundaries. These assumptions define the problem to be symmetric with regard to the x-axis. With these simplifications some very important

features of the motion of this system can be established. (a) A steady-state motion of the whole system is possible indeed. (b) The dimensionless criterion Λ:

$$\Lambda = \frac{m^{TJ}a}{m^{GB}} = \frac{2\theta}{2\cos\theta - 1} \tag{3}$$

describes the drag influence of the triple junction on the motion of the entire boundary system. For Λ >>1 the junction does not drag the motion of the boundary system, and the angle θ tends to the equilibrium value $\pi/3$. In such a case the velocity v of the motion of the entire boundary system is independent of the mobility of the triple junction and is determined by the grain boundary mobility and the acting driving force:

$$v = \frac{2\pi m^{GB}\sigma}{3a} \tag{4}$$

In contrast, for Λ<<1 the motion of the system is controlled by the motion of the triple junction and the angle θ tends to zero. The velocity depends only on the triple junction mobility and the grain boundary surface tension σ:

$$v = \sigma m^{TJ} \tag{5}$$

Owing to the fact that there are no measurements and no data of triple junction mobility, we cannot even estimate whether the ratio $m^{\mathrm{TJ}}/m^{\mathrm{GB}}$ is finite. On the other hand, in the course of triple junction motion the straight grain boundary (Fig. 2, GB III) has to be extended. The velocity of its formation is unknown, but the kinetics of it should depend on the structure and properties of the generated grain boundary. Insofar as the rate of formation of this boundary can be interpreted as the velocity of the triple junction, which is proportional to its mobility according to equation (5). In the following a boundary system as shown in Fig. 2 with two identical curved boundaries (GB I and II) and a di€erent straight boundary (GB III) will be considered. The respective surface tensions and the mobilities of the boundaries are:

$$\sigma 1 = \sigma 2 \equiv \sigma \neq \sigma 3, m_1^{GB} = m_2^{GB} \equiv m^{GB} \neq m_3^{GB} \tag{6}$$

In this case the shape of a steadily moving boundary system can be expressed by the equation

$$\frac{d^2y}{dx^2} = -\frac{v}{m^{GB}\sigma}\frac{dy}{dx}\left[1 + \left(\frac{dy}{dx}\right)^2\right] \tag{7}$$

with the boundary conditions

$$y(0) = 0, y(\infty) = \frac{a}{2}, y'(0) = \tan\theta \tag{8}$$

as obvious from Fig. 2. Equations (6)-(8) completely define the problem. The shape of the stationary moving grain boundaries GB I and II (Fig. 1) is given by:

$$y(x) = \xi arccos\left(e^{-\frac{x}{\xi}+C_1}\right) + C_2, \;\; \xi = \frac{a}{2\theta} \tag{9}$$

$$C_1 = \frac{1}{2}ln(\sin\theta)^2, C_2 = \xi\left(\frac{\pi}{2} - \theta\right) \tag{10}$$

The steady-state velocity of GB I and II is

$$v^{GB} = \frac{2\theta m^{GB}\sigma}{a} \tag{11}$$

The velocity of the triple junction v^{TJ} can be expressed as (Soraes, et al., 1941), (Galina, et al., 1987), (Fradkov, et al., 1988):

$$v^{TJ} = m^{TJ} \sum \sigma_i \vec{\tau_i} \tag{12}$$

where every $\vec{\tau_i}$ is the unit vector normal to the triple line and aligned with the plane of the adjacent boundary. If the angles at the triple junction are in equilibrium, the driving force is equal to zero and for a finite triple junction mobility the velocity v^{TJ} should vanish as well. Consequently, for a finite m^{TJ}, the motion of the triple junction disturbs the equilibrium of the angles and, as a result, drags the motion of the boundaries. For the situation given in Fig. 2.

$$v^{TJ} = m^{TJ}(2\sigma \cos\theta - \sigma_3) \tag{13}$$

In the case of steady-state motion of the entire boundary system the velocity of the triple junction equals the velocity of the grain boundaries. Therefore, the steady-state value of the angle θ is determined by equations (11) and (12):

$$\frac{2\theta}{2\cos\theta - \frac{\sigma_3}{\sigma}} = \frac{m^{TJ}a}{m^{GB}} = \Lambda \tag{14}$$

The dimensionless criterion Λ reflects the drag influence of the triple junction on the migration of the system. One can distinguish two limiting cases:

$\Lambda \rightarrow 0$: In this case the angle θ tends to zero, i.e. the motion of the entire boundary system is governed by the mobility of the triple junction and the corresponding driving force. For the limit $\theta = 0^{o}$ the velocity of the system is given with equation (13) by

$$v = m^{TJ}(2\sigma - \sigma_3) \tag{15}$$

$\Lambda \rightarrow \infty$: In this case the angle θ tends to the value of thermodynamic equilibrium:

$$\theta = arccos\left(\frac{\sigma_3}{2\sigma}\right) = \theta_{eq.} \tag{16}$$

The motion of the system is independent of the triple junction mobility and is governed only by the grain boundary mobility and the corresponding driving force. The velocity of the boundary system in this case with equations (11) and (16) is given by:

$$v = \frac{2\theta_{eq} m_{GB\sigma}}{a} \tag{17}$$

The two states of motion of the entire grain boundary system can be distinguished experimentally for a known ratio $\sigma 3/\sigma$ by measuring the contact angle θ.

5. Influence of external shear stresses on grain boundary migration

A method to activate and investigate the migration of planar, symmetrical tilt boundaries is influenced by external shear stress. It is shown that low- as well as high-angle boundaries could be moved by this shear stress. From the activation parameters for grain boundary migration, the transition from low- to high-angle boundaries can be determined. The migration kinetics were compared with results on curved boundaries, and it was shown that

the kinetics of stress induced motion were different from the migration kinetics of curvature driven boundaries. Washburn, et al. 1952 and Li, et al., 1953 investigated planar low-angle boundaries in Zn under the influence of an external shear stress and observed the motion with polarized light in an optical microscope. Symmetrical low angle tilt boundaries consist of periodic arrangements of a single sets of edge dislocations. An external shear stress perpendicular to the boundary plane will cause a force on each dislocation and in summary a driving force on the boundary. The samples were exposed to a shear stress ranging from 10^{-1} to 10^{-3}MPa. In aluminum (purity 99.999%) the yield stress is 15–20MPa, hence the applied shear stress is definitely in the elastic range. High angle symmetrical tilt boundaries also can be formally described as an arrangement of a single set of edge dislocations except that the dislocation cores overlap and the identity of the dislocations gets lost in the relaxed boundary structure. I showed that irrespective of the magnitude of the angle of rotation, grain boundaries can be moved under the action of the applied shear stress. The transition from low- to high-angle grain boundaries is revealed by a conspicuous step of the activation enthalpy at a misorientation angle of 13.6°. This holds for low angle as well as for high angle symmetrical tilt boundaries. For the curvature driven grain boundaries our results are in good agreement with previous experimental data [14] and one can see a strong dependency of the activation enthalpy on the misorientation angle, i.e. on the grain boundary structure. There is also a clear difference between the activation enthalpies for the stress induced motion of the planar high angle grain boundaries and the curvature driven migration of the curved high angle grain boundaries. Obviously, a dislocation in a high angle grain boundary does not relax completely its strain field and correspondingly, a biased elastic energy density induced by an applied shear stress will induce a force on all dislocations that comprise the grain boundary. The results prove that grain boundaries can be driven by an applied shear stress irrespective whether low- or high-angle boundaries. Obviously, the motion of the grain boundary is caused by the movement of the dislocations, which compose the grain boundary. The motion of an edge dislocation in a FCC crystal in reaction to an applied shear stress ought to be purely mechanical and not thermally activated. Obviously, the observed grain boundary motion is a thermally activated process controlled by diffusion. To understand this, one has to recognize first that grain boundary motion is a drift motion since it experiences a driving force that is smaller compared with thermal energy. Moreover, real boundaries are never perfect symmetrical tilt boundaries but always contain structural dislocations of other Burgers vectors. These dislocations have to be displaced by nonconservative motion to make the entire boundary migrate. The climb process requires diffusion, which can only be volume diffusion for low angle grain boundaries but grain boundary diffusion for high angle grain boundaries according to the observed activation enthalpies. The different behavior of curvature driven grain boundaries is not due to the curvature of the boundaries rather than due to a different effect of the respective driving force. While an applied shear stress couples with the dislocation content of the boundary in a curved grain boundary each individual atom experiences a drift pressure to move in order to reduce curvature.

6. Shape of the moving grain boundaries

The principal parameter which controls the motion of a grain boundary is the grain boundary mobility. In practically all relevant cases the motion of a straight grain boundary is the exception rather than the rule. That is why the shape of a moving grain boundary is of

interest and it will be shown that the grain boundary shape is a source of new interesting and useful findings of grain boundary motion, for the interaction of a moving grain boundary with mobile particles, in particular. The experimentally derived shape of grain boundary 'quarter-loop' in Al-bicrystals of different purity was compared with theoretical calculations in the Lücke–Detert approximation. The shape of a moving GB quarter-loop was determined analytically under the assumption of uniform GB properties and quasi-two-dimensionality (Verhasselt, et al., 1999):

$$y(x) = \{-(b_F - b_L)arccos\left(\frac{\sin\Theta}{e^{x^*/b_F}}\right) + \frac{a}{2} - b_L\frac{\pi}{2} + b_F arccos\left(e^{b_F ln(\sin\Theta) - x/b_F}\right)$$

$$0 \le x \le x^*\frac{a}{2} - b_L\frac{\pi}{2} + b_L arccos\left(e^{b_L \ln(\sin\Theta) - x^*\left((b_L/b_F)-1\right) - x/b_L}\right) \tag{18}$$

$$x \ge x^*$$

where b_L is:

$$b_L = \frac{b_F\left(arc\,cos\left(\sin\Theta/e^{x^*/b_F} + \Theta - (\pi/2) - a/2\right)\right)}{arc\,cos\left(\sin\Theta/e^{x^*/b_F}\right) - (\pi/2)}b \tag{19}$$

The parameters in Eq. (18) are the width of the shrinking grain $a/2$, the angle Θ of the grain boundary with the free surfaces in the triple junction, the critical point x^*, and b_F and b_L: $b_L = m_L\sigma/V$; $b_F = m_F\sigma/V$, where m_L and m_F are the GB mobilities for 'loaded' and 'free' GB, respectively, σ is GB surface tension, V is a velocity of a quarter-loop. The first two parameters can be measured directly in the experiment. The latter two have to be chosen in an approximate way to fit the experimentally derived grain boundary shape. The point x^* is the point of intersection 'free' and 'loaded' segments of the GB. The value m_L/m_F is a measure for how drastic the change between the 'free' and the 'loaded' part in the point of intersection will be. The investigation proves that the influence of the impurity atoms on grain boundary properties and behavior is rather strong even in very pure materials. As mentioned above, the shape of a moving grain boundary is a new source of information on grain boundary migration. One example is given in Fig. 4, where the value of the critical distance x^*, normalized by the driving force (in terms of the quarter-loop width a) is plotted versus the impurity content. In accordance with the Lücke–Detert theory the critical velocity v^* (and rigidly bound to it the position of the critical point x^* on the quarter-loop) is determined by the balance between the maximum force of interaction of the impurity atoms with the boundary and the force, which is imposed by the energy dissipation caused by boundary motion across the matrix. The difference of the impurity drag for grain boundaries in samples with different amount of impurities is caused by the adsorption of impurities at the grain boundary. According to theory, the velocity should decrease proportionally to the inverse of the concentration of adsorbed atoms. Therefore x^* should increase with decreasing impurity content, as observed qualitatively (Fig. 4 and Fig. 5). However, a linear relation between the inverse of the impurity concentration and v^*, i.e. x^*, is not observed over the whole concentration range, which indicates a more complicated interaction of adsorbed atoms with the grain boundary. In such a case, x^*/a should increase more strongly with decreasing impurity content than it does linearly. This tendency is indeed observed (Fig. 4 and Fig. 5).

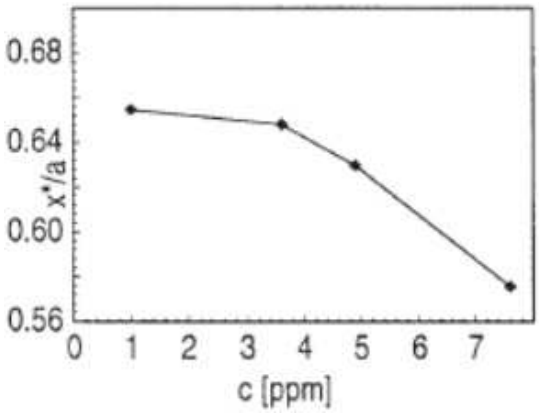

Fig. 4. Dependence of critical point x^*/a on impurity content; (b) reciprocal impurity content (From: Shvindlerman, Gottstein, 2001).

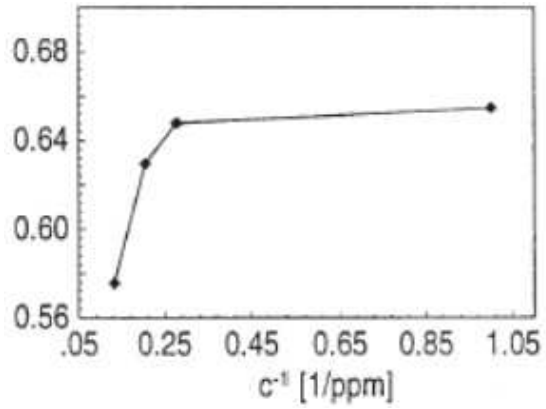

Fig. 5. Dependence of critical point x^*/a on reciprocal impurity content (From: Shvindlerman, Gottstein, 2001).

7. Dragging effect of tripe junction on grain boundary motion

In spite of the fact that a line (or column) of intersection of three boundaries constitutes a system with specific thermodynamic properties was realized more than 100 years ago (by Gibbs), the kinetic properties of this subject, in particular the mobility of triple junctions, and their influence on grain growth and relevant processes were ignored up to now. Although the number of triple junctions in polycrystals is comparable in magnitude with the number of boundaries, all peculiarities in the behavior of polycrystals during grain growth were solely attributed to the motion of grain boundaries so far. It was tacitly assumed in theoretical approaches, computer simulations and interpretation of experiment results that triple junctions do not disturb grain boundary motion and that their role in grain growth is reduced to preserve the thermodynamically prescribed equilibrium angles at the lines (or the points for 2-D systems) where boundaries meet. The most prominent example of how

this assumption determines the fundamental concepts of grain structure evolution gives the Von Neumann–Mullins relation (Neumann, 1952 and Mullins, 1956). No doubt this relation forms the basis for practically all theoretical and experimental investigations as well as computer simulations of microstructure evolution in 2-D polycrystals in the course of grain growth. This relation is based on three essential assumptions, namely, (i) all grain boundaries possess equal mobilities and surface tensions, irrespective of their misorientation and crystallographic orientation of the boundaries; (ii) the mobility of a grain boundary is independent of its velocity; (iii) the third assumption relates directly to the triple junctions, namely, they do not affect grain boundary motion; therefore, the contact angles at triple junctions are in equilibrium and, due to the first assumption, are equal to 120°. As it was shown in (Neumann, 1952 and Mullins, 1956), for 2-D grain, the rate of change of the grain area S can be expressed by:

$$\frac{dS}{dt} = -A_b \oint d\varphi \tag{20}$$

where $A_b = m_b\sigma$; m_b being the grain boundary mobility, σ is the grain boundary surface tension. If the grain were bordered by a smooth line, the integral in Eq. (20) would equal 2π. However, owing to the discontinuous angular change at every triple junction, the angular interval $\Delta\varphi=\pi/3$ is subtracted from the total value of 2 π for each triple junction. Consequently:

$$\frac{dS}{dt} = -A_b\left(2\pi - \frac{n\pi}{3}\right) = \frac{A_b\pi}{3}(n-6) \tag{21}$$

where n is the number of triple junctions for each respective grain, i.e. the topological class of the grain.

8. Conclusions

Many researchers have used the two-step sintering as a design process to obtain samples with a microstcture without grain growth in final stage of sintering. Same exemples that we can cite are:

- Chen, I.W. & Wang, X.H. (2000) obtained samples of the Y_2O_3 with a grain size of 60nm can be prepared by a simple two-step sintering method, at temperatures of about 1,000ºC without applied pressure. The suppression of the final-stage grain growth is achieved by exploiting the difference in kinetics between grain boundary diffusion and grain-boundary migration. Such a process should facilitate the cost-effective preparation of other nanocrystalline materials for practical applications.
- 2: Lapa, et al., (2009) prepared samples of the yttrium and gadolinium-doped ceria-based electrolytes (20 at% dopant cation) with and without small Ga_2O_3-additions (0.5 mol%). The average grain sizes in the range 150–250 nm and densifications up to about 94% were found dependent on the sintering profile and presence of Ga. The grain boundary arcs in the impedance spectra increased significantly with Ga-doping, cancelling the apparently positive role of Ga on bulk transport, evidenced mostly in the case of yttrium-doped materials.
- 3: Wang, et al. (2006) used two-step sintering to sinter $BaTiO_3$ and Ni–Cu–Zn ferrite ceramics to high density with unprecedentedly fine grain size, by suppressing grain

growth in the final stage of densification. Dense $BaTiO_3$ ceramics with a grain size of 35 nm undergo distortions from cubic to various low-temperature ferroelectric structures. Dense fine grain Ni–Cu–Zn ferrite ceramics have the same saturation magnetization as their coarse grain counterparts.

9. Acknowledgment

The authors wish to thank PRH-ANP, CAPES, LMCME-UFRN, Materials Laboratory-UFRN and NEPGN-UFRN.

10. References

Arzt, E., Ashby, M. F. & Verrall, R. A. (1993) Interface-controlled diffusional creep. Acta Metall. 31, 1977± 1989.

Cannon, R. M., Rhodes, W. H. & Heuer, A. H. (1980) Plastic deformation of fine-grained alumina: I. interface-controlled diffusional creep. J. Am. Ceram. Soc. 63, 48-53

Chen, I.W. (1993). Mobility control of ceramic grain boundaries and interfaces, Materials Science and Engineering. 166. 51-58.

Chen, I.W. (2000). Grain boundary kinectics in oxide ceramics with the cubic fluorite crystal structure and its derivates. Interface Science. Vol. 8. Pp. 147-156.

Chen, I.W. & Wang, X.H. (2000). Sintering dense nanocrystaline ceramics without final-stage grain growth. Nature. Vol. 404.

Chen, I.W. & Xue, L.A. (1990). Development of superplastic structure ceramics. Journal of American Ceramics Society. Vol. 73.

Chen, P.L. & Chen, I.W. (1997). Journal of American Ceramics Society.

Coble, R.L. (1965). Intermediate-stage sintering : Modification and correction of a lattice-diffusion model. Vol. 36.

Czubayko, L., Sursaeva, V. G., Gottstein, G. & Shvindlerman, L. S., (1998) Influence of triple junctions on grain boundary motion. Acta Mater. 46, 5863±5871.

Galina, A. V., Fradkov, V. E. and Shvindlerman, L. S., (1987) Physics Metals Metallogr., 63, 165.

Herring, C. (1950). Effect of change of scale on sintering phenomena. Journal Applied to Physics. Vol. 21.

Herring, C. (1951). The physics of powder metallurgy. McGraw-Hill. New York. Pp. 143.

Hesabi, Z.R. ; Haghighatzadeh, M. ; Mazaheri, M. ; Galusek, D.S.K. & Sadrnezhaad. (2008) Suppression of grain growth in sub-micrometer alumina via two-step sintering method. Journal of the European Ceramic Society.

Jonghe, L.C. ; Rahaman, M.N. (2003). Sinterig ceramics. Handbook of Advanced Ceramics.

Land, T. A., Martin, T. L., Potapenko, S., Palmore, G. T. & De Yoreo, J. J. (1999) Recovery of surfaces from impurity poisoning during crystal growth. Nature 399, 442±445.

Lapa, C.M. ; Souza, D.P. ; Figueiredo, F.M.L. & Marques, F.M.B. (2009). Electrical and microstructural characterization of two-step sintered ceria based electrolytes. Journal of Power Sources. Vol. 187. Pp. 204-208.

Lapa, C.M. ; Souza, D.P. ; Figueiredo, F.M.L. & Marques, F.M.B. (2009). Two-step sintering ceria-based electrolytes. International Journal of Hydrogen Energy. Pp. 1-5.

Li, C.H., Edwards, E.H., Washburn, J., Parker, E.R., (1954) Recent observations on the motion of small angle dislocation boundaries Acta Met. 2, 322–333.

Mullins, W.W.,(1956), Two-dimensional motion of idealized grain boundaries. J. Appl. Phys. 27, 900–904.

Fathi, M.H.; Kharaziha, M. (2009). Two-step sintering of dense, nanostructural forsterite. Materials Letters - 63, Pp. 1455–1458.

Fradkov, V. E. and Shvindlerman, L. S., (1988) Structure and Properties of Interfaces in Metals. Nauka, Moscow, p. 213.

McFadden, S.X. ; Mishra, R.S. ; Valiev, R.Z. ; Zhilyaev, A.P. & Mukherjee, A.K. (1999). Low-temperature superplasticity in nanostructured nickel and metal alloys. Nature. Vol. 396. Pp. 684-686.

Robert, C.L. ; Ansart, F. ; Degolet, C.L. ; Gaudon, M. & Rousset, A. (2003). Dense yttria stabilized zirconia: sintering and microstructure Ceramics International. Vol. 29. Pp. 151-158.

Shahraki, M.M.; Shojaee, S.A.; Sani, M.A.D.; Nemati, A. & Safaee, I. (2010). Two-step sintering of ZnO varistors. Solid State Ionics.

Shvindlerman, L.S., Gottstein, G., (2001), Grain boundary and triple junction migration Materials Science and Engineering, A302, 141–150.

Soraes, A., Ferro, A. C. and Fortes, M. A., (1941) Scripta metallurgycal., 1985, 19.

Swinkels, F.B. & Ashby M.F. (1981). Acta Metallurgycal. Vol. 29. Pp. 259.

Verhasselt, J.C., Gottstein, G., Molodov, D.A., Shvindlerman, L.S., (1999) Acta Mater. 47, 887–892.

Von Neumann, J., (1952) in: Metal Interfaces, American Society for Testing Materials, Cleveland, OH, P. 108.

Wakai, F. et al. (1990) A superplastic covalent crystal composite. Nature. Vol. 344.

Wang, J.C.; Huang, C.Y.; Wu, Y.C. (2008) Two-step sintering of fine alumina-zirconia ceramics. Ceramics international.

Wang, X.H. ; Chen, P.L. & Chen, I.W. (2006). Two-step sintering of ceramics with constant grain-size, I Y_2O_3. Journal American Ceramics Society. Vol. 89. Pp. 431-437.

Wang, X.H.; Deng, X.Y.; Bai, H.L.; Zhou H.; Qu, W.G. & Li, L.T. (2006). Two-step sintering of ceramics with constant grain-size, II BaTiO3 and Ni-Cu-Zn ferrite. Journal American Ceramics Society.Vol. 89. 438-443.

Washburn, J., Parker,E.R., J. (1952), Journal of Metals. 4, 1076–1078.

Winning, M., Gottstein,G., Shvindlerman, L.S., in: T. Sakai, G. Suzuki (Eds.), (1999), Recrystallization and Related Phenomena, The Japan Institute of Metals, pp. 451–456.

Wright, G.J. (2008). Constrained sintering of yttria-stabilized zirconia electrolytes: The influence of two-step sintering profiles on microstructure and gas permeance. International Journal Applied to Ceramic Technologies. Vol. 5. Pp. 589-596.

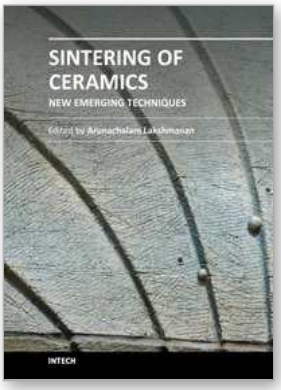

Sintering of Ceramics - New Emerging Techniques
Edited by Dr. Arunachalam Lakshmanan

ISBN 978-953-51-0017-1
Hard cover, 610 pages
Publisher InTech
Published online 02, March, 2012
Published in print edition March, 2012

The chapters covered in this book include emerging new techniques on sintering. Major experts in this field contributed to this book and presented their research. Topics covered in this publication include Spark plasma sintering, Magnetic Pulsed compaction, Low Temperature Co-fired Ceramic technology for the preparation of 3-dimesinal circuits, Microwave sintering of thermistor ceramics, Synthesis of Bio-compatible ceramics, Sintering of Rare Earth Doped Bismuth Titanate Ceramics prepared by Soft Combustion, nanostructured ceramics, alternative solid-state reaction routes yielding densified bulk ceramics and nanopowders, Sintering of intermetallic superconductors such as MgB2, impurity doping in luminescence phosphors synthesized using soft techniques, etc. Other advanced sintering techniques such as radiation thermal sintering for the manufacture of thin film solid oxide fuel cells are also described.

INTECH
open science | open minds

InTech Europe
University Campus STeP Ri
Slavka Krautzeka 83/A
51000 Rijeka, Croatia
Phone: +385 (51) 770 447
Fax: +385 (51) 686 166
www.intechopen.com

InTech China
Unit 405, Office Block, Hotel Equatorial Shanghai
No.65, Yan An Road (West), Shanghai, 200040, China
中国上海市延安西路65号上海国际贵都大饭店办公楼405单元
Phone: +86-21-62489820
Fax: +86-21-62489821